Journal of Magnetism and Magnetic Materials 474 (2019) 355–364

Contents lists available at ScienceDirect

Journal of Magnetism and Magnetic Materials

journal homepage: www.elsevier.com/locate/jmmm

Research articles

Hyaluronic acid modified bubble-generating magnetic liposomes for targeted delivery of doxorubicin

Gils Jose[a], Yu-Jen Lu[b], Huai-An Chen[a], Hao-Lung Hsu[a], Jung-Tung Hung[c], Anilkumar T.S.[a], Jyh-Ping Chen[a,d,e,f,*]

[a] Department of Chemical and Materials Engineering, Chang Gung University, Kwei-San, Taoyuan 33302, Taiwan, ROC
[b] Department of Neurosurgery, Chang Gung Memorial Hospital, Linkou, Kwei-San, Taoyuan 33305, Taiwan, ROC
[c] Institute of Stem Cell & Translational Cancer Research, Chang Gung Memorial Hospital, Linkou, Kwei-San, Taoyuan 33305, Taiwan, ROC
[d] Department of Plastic and Reconstructive Surgery and Craniofacial Research Center, Chang Gung Memorial Hospital, Kwei-San, Taoyuan 33305, Taiwan, ROC
[e] Research Center for Chinese Herbal Medicine and Research Center for Food and Cosmetic Safety, College of Human Ecology, Chang Gung University of Science and Technology, Kwei-San, Taoyuan 33302, Taiwan, ROC
[f] Department of Materials Engineering, Ming Chi University of Technology, New Taipei City 24301, Taiwan, ROC

ARTICLE INFO

Keywords:
Bubble-generating
Hyaluronic acid
Magnetic liposomes
Doxorubicin
Targeted delivery
Cancer therapy

ABSTRACT

The combination of liposomes and magnetic nanoparticles (MNPs) is a promising approach for cancer therapy due to its capability for magnetic field-directed targeted drug delivery at the diseased area. Contemporaneously, bubble-generating liposomes are of great interest in the field of cancer therapy, due to its triggered drug release properties and its ability to rupture cancer cells through cavitation induction. Therefore, the objective of the current study is to develop a bubble-generating magnetic liposomal (BMLs) drug delivery system with triggered drug release properties for targeted delivery of doxorubicin (DOX) in cancer therapy. Citric acid-coated iron oxide MNPs was co-entrapped with ammonium bicarbonate to produce BMLs by lipid film hydration method. BMLs were further modified by coating hyaluronic acid-polyethylene glycol (HA-PEG) on liposome surface to produce HA-PEG-BMLs for ligand-mediated active targeting of tumor cells. The resultant liposomes were found to be spherical in shape with an average particle size ranging from 100 to 170 nm. The physico-chemical properties and bubble-generating properties of liposomes were studied. In vitro drug release studies showed enhanced drug release under hyperthermia condition (43 °C) from BMLs/DOX and HA-PEG-BMLs/DOX due to more intense CO_2 bubbles generation with faster decomposition rates of co-entrapped ammonium bicarbonate. In vitro cell culture studies using human glioblastoma cells (U87) were performed to evaluate the targeting efficiencies and anti-tumor efficacy of DOX-loaded liposomes. Magnetic targeted delivery of DOX was also demonstrated from LIVE/DEAD cell viability assays. The confocal microscopy and flow cytometry analysis confirmed enhanced intracellular uptake of HA-PEG-BMLs by U87 though binding of HA to overexpressed CD44 receptors on cell surface, which facilitated internalization of HA-PEG-BMLs/DOX through endocytosis and resulted in elevated DOX concentration in cancer cells. The combination of elevated intracellular DOX concentration and triggered DOX release at 43 °C led to enhanced cytotoxicity toward U87 cells in vitro. Thus, HA-PEG-BMLs will be useful for hyperthermia-induced targeted delivery of DOX for cancer therapy.

1. Introduction

Undoubtedly, cancer is one of the deadliest diseases in human history. In defiance of the role played by conventional chemotherapy in elevating the lifespan of many cancer sufferers, the vague distribution of therapeutics and limited bioavailability engendered to significant toxicity towards healthy tissues and to inefficacious therapy [1]. Within all nanometer-scale systems used to deliver chemical drugs, genes, vaccines, and imaging agents, the liposomal system was found to be one of the most effective delivery systems, due to its capability to transport the therapeutics by overcoming physiological barriers, and to release the cargo at maximum concentration to the diseased area [2–4]. Contemporaneously, bubble-generating liposomes are of great interest in the field of cancer therapy, due to its triggered drug release properties [5]. Also, utilizing its tendency to cause cavitation during bubble formation, which involves either rapid growth followed by the collapse of

* Corresponding author at: 259 Wen-Hwa 1st Road, Kwei-San, Taoyuan 33302, Taiwan, ROC.
E-mail address: jpchen@mail.cgu.edu.tw (J.-P. Chen).

https://doi.org/10.1016/j.jmmm.2018.11.019
Received 24 June 2018; Received in revised form 26 October 2018; Accepted 4 November 2018
Available online 05 November 2018
0304-8853/

bubbles or sustained oscillatory motion of bubbles, bubble-generating liposomes also have the capability to rupture cancer cells [6]. This cavitation produces shock waves or high velocity micro jets that in turn damage the tissues physically, chemically and biologically, leaving other cells unscathed.

Liposomes are imperceptible particles composed of self-assembled lipid molecules having hydrophilic head group and hydrophobic tail, which exist either as unilamellar vesicle with one lipid bilayer enclosing a single aqueous compartment or as multilamellar vesicles with a number of concentric bilayers enclosing equal number of aqueous spaces [7,8]. Because of the amphipathic nature of lipids, these vesicles with one or more phospholipid bilayer membranes can carry both hydrophilic and hydrophobic drugs, depending on the nature of those drugs [4,9]. The application of magnetic nanoparticles (MNPs) in guiding drugs and nanoparticles to the tissue or organ with the help of an external magnetic field has been discussed before [10]. On the other hand, it is also possible to produce magnetic liposomes by encapsulated MNPs within aqueous cores of liposomes, which can offer multiple functions including in vivo guidance, contrast enhancement of MRI imaging and localized hyperthermia [11–13].

Although nanocarriers are considered to be efficient as carriers for chemotherapeutic drugs, a more efficient outcome of cancer therapy could be fulfilled by using targeted drug delivery, where most of the administered drug will be guided to the targeted site to eliminate or minimize the accumulation of the drug at any non-targeted sites [14]. This could be achieved through the modification of nanocarriers so that they can be directed by a magnetic field or by ligand-receptor interactions, which would result in active tumor targeting after extravasation [15]. Indeed, using the ligand-mediated internalization, which is attained through the binding of certain ligands to their receptors on cancer cell surface, internalization of drug-loaded nanocarriers into cancer cells could lead to higher intracellular drug concentrations and raise cancer cell killing efficacy [16]. Among ligands considered for tumor targeting, hyaluronic acid (HA) could be recognized by the CD44 receptor that is overexpressed on the surface of many types of cancer cells, including glioblastoma cells [17,18]. In this way, a more significant therapeutic outcome for brain tumor therapy could be expected through enhanced internalization of drug-loaded HA-modified magnetic liposomes through active targeting to glioblastoma cells.

In this study, we first prepared bubble-generating magnetic liposomes (BMLs) loaded with citric acid-coated magnetic nanoparticles (CMNPs) and further modified them with hyaluronic acid-polyethylene glycol (HA-PEG) to prepare a dual targeted nano-vehicle (HA-PEG-BMLs) for doxorubicin (DOX) delivery. We expect that after the liposomes were internalized by cancer cells, they can be thermally triggered at 43 °C to generate CO_2 bubbles, which can produce a disruptive force to disrupt the lipid bilayer membrane, followed by DOX release and death of cancer cells. Therefore, we tested the hypothesis that HA-PEG-BMLs/DOX could show chemotherapeutic accumulation and increased cytotoxicity to U87 human glioblastoma cells in vitro.

2. Materials and method

2.1. Materials

Fe(II) chloride tetrahydate (99%) and Fe(III) chloride hexahydrate (97%) were acquired from Acros Organics. 1,2-Distearoyl-*sn*-glycero-3-phosphocholine (DSPC) was purchased from Avanti Polar Lipids. Cholesterol, dimethyldioctadecylammonium bromide (DDAB) and Triton X-100 were purchased from Sigma-Aldrich. Hyaluronic acid (HA) in the form of sodium hyaluronate (M.W. = 1.3×10^6 Da) was purchased from Shandong Freda Biochem. Co. Methoxy polyethylene glycol amine (MPEG-NH_2, M.W. = 5000 Da) was obtained from Alfa Aesar. CdSSe/ZnS Quantum Dots with amine end groups (QDs-NH_2) was a product of Ocean NanoTech. Doxorubicin (hydrochloride salt) was acquired from LC Laboratories. Reagent grade chemicals were used for all experiments without further purification.

2.2. Synthesis of citric acid-coated iron oxide magnetic nanoparticles (CMNPs)

The CMNPs were prepared by the co-precipitation method as described before [19,20]. For this, 0.875 g of $FeCl_2{\cdot}4H_2O$ and 2.375 g of $FeCl_3{\cdot}6H_2O$ were mixed in 40 mL of double-distilled water (DDI water) in a three-neck flask. The mixture was heated to 70 °C with constant stirring at 100 rpm under nitrogen atmosphere. Subsequently, the temperature and rotation speed were increased to 90 °C and 1150 rpm, and 5 mL of 25% NH_4OH solution was added to the mixture. Two milliliters of citric acid solution (0.5*g*/ml) was then added using a syringe, and the reaction was continued for another 90 min at 1150 rpm. The black-colored colloidal CMNPs obtained were magnetically separated after diluting with DDI water to 1:1 vol ratio. The CMNPs were then dialyzed against DDI water using a hollow fiber module (Spectrum Laboratories) to remove unbound citric acid and NH_4OH.

2.3. Synthesis of hyaluronic acid-polyethylene glycol (HA-PEG)

PEG-grafted hyaluronic acid was synthesized by following the procedure reported before with slight modifications [21]. In brief, 1.2 g of HA was dissolved in 50 mM 2-(N-morpholino)ethanesulfonic acid (MES) buffer. To this solution, equimolar amount of MPEG-NH_2 was added and stirred until complete dissolution. 1-Ethyl-3-(3-dimethylaminopropyl) carbodiimide (EDC, 1 mM) was then added and allowed to react for 2 h at room temperature. The viscous HA-PEG solution obtained was dialyzed against DDI water using a 10 kDa MWCO dialysis tubing for 48 h at room temperature to remove unreacted MPEG-NH_2.

2.4. Preparation of liposomes

The bubble-generating magnetic liposomes (BMLs) were prepared in the phosphate buffered saline (PBS) containing NH_4HCO_3 using the thin film hydration method [20]. DSPC, cholesterol and DDAB (molar ratio 6:4:1) were mixed in a 100 mL round-bottom flask and dissolved in 2:1(v/v) mixture of chloroform/methanol solution. 1.5 mL of this solution was then roto-evaporated (EYELA N- 1200AVF, Japan) at 100 psi and 55 °C for 20 min, and kept in the vacuum oven overnight, to remove the organic solvent completely and to form the lipid film. The phospholipid film so obtained on the wall of the round-bottom flask was hydrated with 10 mL PBS solution containing 2 M NH_4HCO_3 and 0.2 mg/ml CMNPs for 20 min at 20 °C. The suspension obtained after the hydration process was sonicated using Q700 sonicator (Qsonica) for 20 min at 30% amplitude with 5 s pulse on/off cycles. This was followed with centrifugation at 1000*g* for 5 min to remove the un-encapsulated CMNPs. To remove the excess NH_4HCO_3, the liposomes were dialyzed against 10 wt% sucrose solution containing 5 mM NaCl for 24 h, and again centrifuged for 30 min at 60000*g* using a high speed centrifuge (Hermle Z36HK). Blank liposomes without NH_4HCO_3 and CMNPs were prepared using the same procedure but replacing the hydration solution with PBS. To prepare HA-PEG-BMLs, BMLs was modified with HA-PEG though the electrostatic interaction between cationic liposomal surface (due to the presence of DDAB) and negatively charged HA-PEG. Briefly, HA-PEG solution (1 mg/mL) was added drop-wisely to an equal volume of BMLs solution (1 mg/ml) under stirring at 4 °C for 30 min. The resulting solution was centrifuged at 60000*g* for 30 min to remove the free HA-PEG, and modified liposomes were re-suspended in DDI water.

2.5. DOX loading in liposomes

The remote loading technique using the *trans*-membrane gradients is applied to achieve an optimum intra-liposome concentrations of DOX

[22]. After the un-encapsulated NH_4HCO_3 is removed via dialysis, some of the encapsulated ammonium (NH_4^+) ions undergo dissociation to form protons (H^+) and ammonia (NH_3), and the resultant ammonia molecules rapidly cross the liposomal membrane, which leaves free protons trapped in the liposome because of their low membrane permeability. At this stage, DOX was added to the liposome suspension in different lipid/drug ratio (1: 0.01, 1: 0.05, 1: 0.1 and 1: 0.15) and allowed it to mix well at room temperature for 4 h. When the un-protonated DOX enters the proton-rich aqueous layer of the liposome by diffusion, it becomes protonated and reacts with bicarbonate ions to form DOX-bicarbonate salt. In this way, drug in the outer aqueous phase was encapsulated into the liposome and precipitated in the inner phase to achieve better penetration of drug into the liposome. Once the drug was encapsulated into the liposome, the suspension was centrifuged at 60000*g* for 30 min to remove un-encapsulated DOX from the liposome suspension. The DOX-loaded liposomes (BMLs/DOX and HA-PEG-BMLs/DOX) obtained after three-time centrifugation was re-suspended in DDI water. The encapsulation efficiency (EE) and loading efficiency (LE) of DOX in liposomes was calculated using the following equations.

$$\text{Encapsulation efficiency (\%)} = \frac{\text{Weightof encapsulated DOX}}{\text{Total weight of DOX}} \times 100 \quad (1)$$

$$\text{Loading efficiency (\%)} = \frac{\text{Weight of encapsulated DOX}}{\text{Weight of liposomes}} \times 100 \quad (2)$$

2.6. Physico-chemical characterization

The morphology of the prepared samples was analyzed using a transmission electron microscope (TEM, JEOL JEM2000 EX II) at an acceleration voltage of 100 kV. The particle size and zeta potential was detected by dynamic light scattering (DLS) using a Zetasizer (Nano ZS 90, Malvern, UK) by suspending the sample in distilled deionized water. Thermal behavior and the encapsulation of Fe_3O_4 MNPs into the liposomes were determined by thermogravimetric analysis (TGA) using Q50 TGA (TA instruments, New Castle, USA) with 10 mg freeze-dried samples in a platinum pan under nitrogen atmosphere from 50 to 700 °C. The nominal nitrogen flow rate and the heating rate were maintained at 60 mL/min and 10 °C/min, respectively. The Fe_3O_4 loading was further confirmed by inductively coupled plasma mass spectrometry (ICP, Varian 710-ES). A superconducting quantum interference device magnetometer (SQUID, Quantum Design MPMS-3) at 25 °C and ± 10,000G applied magnetic field was used to measure the magnetization of samples. Bubble generation in the liposomes, after decomposition of encapsulated NH_4HCO_3, was visualized by a portable ultrasound imaging system (Terason t3200). For the characterization of chemical compounds using Fourier transform infrared spectroscopy (FTIR, Horiba FT-730 spectrometer), the samples were blended with KBr and then compressed to form a pellet.

2.7. DOX release from liposomes

The temperature-dependent drug release properties of the liposomes were analyzed by incubating BMLs/DOX or HA-PEG-BMLs/DOX in 1 mL PBS (pH 7.4) at 37 °C for 24 h [23]. Hyperthermia-induced drug release was studied by immersing the sample at 43 °C for 24 h. At specific times, all PBS was removed and replenished with equal volume of fresh PBS. The concentration of DOX in PBS was determined at 490 nm using a UV–visible spectrophotometer (UV-1700, Shimadzu, Kyoto, Japan). The accumulative drug release percentage was calculated from the total weight of encapsulated DOX after incubating drug-loaded liposomes in lysis buffer (0.1% Triton X-100 in PBS, pH 7.4) for 30 min at 37 °C.

2.8. Intracellular uptake

To evaluate the effect of HA-PEG coating on intracellular uptake qualitatively, U87 cells seeded in 24-well cell culture plate at 5×10^4 cells/well were treated with quantum dots (QDs)-labelled liposomes (final concentration of 100 μg/mL liposome in culture medium) for 24 h. The labelling of liposomes was achieved through covalent binding after activating carboxylate groups in liposomes with EDC (5 μM), followed by reacting with QDs-NH_2 for 1 h room temperature. The product was centrifuged at 65000*g* for 30 min to remove unbound reagents from the liposomes. After incubation with QDs-labelled liposomes for 24 h, the cells were washed with PBS and the lysosomes were labeled with LysoTracker Red DND-99 (1 μM, Thermo Fisher Scientific) for 1 h at 37 °C. Labeled cells were fixed with 4% paraformaldehyde and further treated with Triton X-100 (0.1% in PBS). Subsequently, the cell nuclei were counterstained with blue fluorescence-producing Hoechst 33342 (1 μg/mL, Thermo Fisher Scientific) for 15 min. The identification of liposomes was made possible by the green fluorescence signals from QDs-labeled liposomes. To confirm whether the uptake of the HA-PEG-BMLs is specific to CD44 receptor, the uptake study was also performed with U87 cells pretreated with 1 mg/mL free HA to block the CD44 on cell surface before adding HA-PEG-BMLs. Cellular internalization of liposomes was assessed by confocal laser scanning microscopy (Zeiss LSM 510 Meta) at excitation wavelength 350 nm/492 nm/577 nm (blue/green/red) and emission wavelength 451 nm/517 nm/590 nm (blue/green/red). All three fluorescence were visualized individually at its corresponding wavelengths and were then merged together to visualize the cellular internalization of liposomes.

2.9. Flow cytometry analysis

The expression of CD44 surface marker on U87, mouse embryonic fibroblast (MEF) and Lewis lung carcinoma (LLC1) cells were analyzed using flow cytometry. The cells were seeded in T25 tissue culture flasks at 2.5×10^5 cells per flask. After 24 h incubation in a humidified incubator at 37 °C under 5% CO_2 atmosphere, the cells were stained with CD44 mouse monoclonal antibody (Cell Signaling Technology 3570) for 30 min at 4 °C, followed by washing the cells with 2 mL FACS buffer to remove unbound antibody from the cells. After centrifugation (300*g* for 5 min), cells were re-suspended in 0.5 mL FACS buffer and conjugated with goat polyclonal secondary antibody to mouse IgG-H&L(Cy3®), preadsorbed (Abcam ab97035) for 1 h. The cells were washed again twice and the final cell pellet was re-suspended in 500 μL of buffer. Analysis of fluorescence was carried out using the FACS instrument (Attune NxT flow cytometer, Life Technologies, USA) with a 488 nm air-cooled argon laser as the excitation source.

For the analysis of DOX accumulation, U87 cells were seeded in the T-25 tissue culture flasks at 2.5×10^5 cells per flask and incubated at 37 °C under 5% CO_2 atmosphere. After the incubation, cells were treated with free DOX, BMLs/DOX or HA-PEG-BMLs/DOX at the same DOX concentration (10 μg/mL DOX prepared in cell culture medium) for 24 h. Subsequently, the medium was removed; cells were washed twice with PBS, detached from the flask using trypsin–EDTA solution and collected in a tube by centrifugation at 2000*g* for 5 min. The cells were washed again twice and the final cell pellet was re-suspended in 500 μL binding buffer. Analysis of DOX fluorescence was carried out using the FACS instrument (Attune NxT Flow cytometer, Life Technologies, USA) with a 488 nm air-cooled argon laser as the excitation source. Fluorescence from cell-associated DOX was detected using a 550 nm long pass emission filter.

The cell apoptosis studies of U87 cells were conducted with the apoptosis detection kit (Thermo Fischer Scientific) containing fluorescein isothiocyanate-labeled Annexin V (Annexin V-FITC) and propidium iodide (PI). U87 cells were seeded in a six-well plate with a cell density of 5×10^5 cells per well and cultured for 24 h. Followed by this, the cells were treated with blank liposome, BMLs, BMLs/DOX or HA-

PEG-BMLs/DOX, as well as with free DOX of the same DOX concentration (10 μg/mL DOX in medium) for 24 h at 37 °C and 43 °C. After the incubation, the cells were trypsinized, washed with PBS and incubated with Annexin V-FITC for 30 min at room temperature to label the live cells. Subsequently, the samples were incubated with PI for dead cell marking, and further analyzed quantitatively using Sony SA 3800 Spectral cell analyzer.

2.10. Magnetic targeting

To investigate the magnetic targeting effect, U87 cells were seeded in a 24-well cell culture plate at 5×10^4 cells/well. To create a permanent magnetic field, a disk-shaped magnet of 7.5 mm diameter was placed under each well of the culture plate. HA-PEG-BMLs/DOX was added to each well at 0.1 mg/mL and the plate was incubated in a humidified CO_2 incubator at 37 °C under 5% CO_2 atmosphere. After incubation for 24 h, the cells were washed with PBS and stained with LIVE/DEAD Cell Viability Assays kits for mammalian cells and observed under an inverted microscope (Olympus IX-71). A control was used for comparison following the same procedure but without magnetic targeting (without using a magnet). The areas of live (green) and dead (red cells) were analyzed using PAX-it software and the percentage of live and dead cells was calculated to compare cell viability.

2.11. In vitro cytotoxicity

The in vitro cytotoxicity of the prepared samples was determined from MTT assays using 3-(4,5-dimethylthiazol-2-yl)-2,5-diphenyltetrazolium bromide. U87 cells were seeded in 96-well culture plates at a density of 2.5×10^3 cells/well and cultured for 24 h in a humidified CO_2 incubator at 37 °C under 5% CO_2 atmosphere. The pre-incubated cells were then treated with BMLs/DOX or HA-PEG-BMLs/DOX, as well as with free DOX of the same DOX concentration (10 μg/mL DOX in medium) for 24 h at 37 °C and 43 °C. After the treatment, the samples were removed, and cells were incubated with 1 mg/mL MTT in cell culture medium for 4 h followed by adding 0.1 mL dimethyl sulfoxide. The optical density readings were recorded using an ELISA plate reader (BioTek Synergy HT) and normalized to readings of the control at each data point, which was taken as 100%. The biocompatibility of the prepared liposomes was also evaluated using MTT assays in the same way, after incubating the cells with DOX-free liposomes (100 μg/mL BMLs or HA-PEG-BMLs).

2.12. Statistical analysis

All data were reported as mean ± standard deviation (SD) and subjected to one-way analysis of variance (ANOVA) analysis with Tukey's HSD Post Hoc Test by IBM SPSS Statistics Software with p value < 0.05 considered to be statistically significant.

3. Results and discussion

3.1. Preparation and characterization of bubble-generating liposomes

From the TEM micrograph, CMNPs agglomerated as shown in Fig. 1A. Nonetheless, the average size of discrete CMNPs could be estimated from the TEM image to be below 20 nm, which was within the size distribution of superparamagnetic particles [24]. The morphology of BMLs examined under TEM revealed successful encapsulation of spherical-shaped CMNPs in the liposomes (Fig. 1B). From DLS studies, the particle size distribution was in the order of HA-PEG-BMLs > BMLs > CMNPs (Fig. 1C), and zeta potential distribution changed from a negative value for CMNPs to a positive value for BMLs and changed back again to a negative value after HA-PEG coating (Fig. 1D). As shown in Table 1, the DLS measurements showed mean values of hydrodynamic diameters of CMNPs, BMLs and HA-PEG-BMLs to be significantly different at 24 nm, 106 nm and 168 nm, respectively, with the polydispersity index (PDI) values below 0.3 for all samples. Coating with HA-PEG therefore led to increase of liposome size measured by DLS. Electrophoretic mobility measurements indicated the average zeta potential increased from −15.4 mV to 12.0 mV after encapsulating CMNPs in BMLs while the average zeta potential value is −18.5 mV for HA-PEG-BMLs (Table 1). Indeed, the change of zeta potential from a positive value to a negative value illustrates the successful coating of liposome with HA-PEG as BMLs are cationic liposomes with the positively changed lipid DDAB while HA is a negative changed polysaccharide (Fig. 1D).

From the FTIR spectra (Fig. 2A), CMNPs shows characteristic peaks of Fe_3O_4 MNPs at 3420 cm^{-1} (−OH), 1645 cm^{-1} (−NH_2) and 571 cm^{-1} (Fe-O) [25]. The presence of these characteristic peaks along with the characteristic peaks assigned to citric acid, i.e. 3442 cm^{-1} (−OH) and 1394 cm^{-1} (C═O asymmetric stretching on −COOH), confirms the successful synthesis of CMNPs [19]. Nonetheless, the characteristic peak at 1715 cm^{-1} due to C═O stretching of citric acid is not visible in the spectrum of CMNPs. This could indicate complex formation between the carboxylate group of citric acid and the Fe atoms on the magnetite surface, which will result in the shifting of the stretching frequency to a lower value as reported previously [26]. The FTIR spectrum of blank liposomes displays characteristic peaks of symmetric and asymmetric -PO_2 stretching vibrations at 1090 and 1220 cm^{-1}, −CH_2 bending vibrations at 1470 cm^{-1} and symmetric and asymmetric stretching vibrations of the −CH_2 in the acyl chain at around 2850 and 2920 cm^{-1}. All characteristics of blank liposomes are also visible in the spectrum of BMLs with additional peaks of CMNPs, which confirms the encapsulation of CMNPs in BMLs. The surface coating with HA-PEG can be identified from the spectrum of HA-PEG-BMLs, which contains additional peaks due to of HA, including the peaks at 611 cm^{-1} and 1043 cm^{-1} corresponding to the C-O-C stretching, 1411 cm^{-1} from C—O group with C═O combination, and 1616 cm^{-1} due to amide II group, in addition to the peaks associated with BMLs [27].

The XRD patterns of CMNPs shown in Fig. 2B shows characteristics peaks of Fe_3O_4 MNPs at $2\theta = 30.5°, 35.8°, 43.8°, 53.4°, 57.3°$ and 62.9°, which is similar to the values in JCPDS file, No. 19-0629. For HA-PEG-BMLs, the XRD patterns show diffraction peaks of CMNPs and blank liposomes without distinguishable difference in 2θ values, indicating the successful encapsulation of CMNPs in HA-PEG-BMLs without making any significant changes of the crystalline structure. It should be noted that CMNPs peaks are not clearly visible for HA-PEG-BMLs, due to the presence of very high intensity peaks from the lipids.

The TGA curves of CMNPs, blank liposomes, BMLs and HA-PEG-BMLs were analyzed to evaluate the thermal behavior of liposomes as well as the loading percentage of CMNPs in liposomes (Fig. 2C). All samples show small mass loss initially below 200 °C due to the loss of adsorbed CO_2 and water. For CMNPs, there is an additional ~4% weight loss at 700 °C with no observable peak temperature from the DTA curve in the insert of Fig. 2C. From the TGA/DTA curve of blank liposomes, a substantial weigh loss is observed when the temperature was increased to 240 °C and peak decomposition temperatures are observed at ~270 °C and ~330 °C with a residual weight of ~95% at 700 °C. For HA-PEG-BMLs, the TGA/DTA curve shows a similar trend as blank liposomes with an additional smaller decomposition peak temperature shown as a shoulder in the DTA curve at 230 °C, which can be ascribed to the decomposition of HA in HA-PEG. From the difference between the residual weight of HA-PEG-BMLs and blank liposomes at 700 °C, the weight percentage of CMNPs in HA-PEG-BMLs could be estimated to be ~26%. The results obtained from the inductively coupled plasma mass spectrometry (ICP) analysis also showed 25% Fe_3O_4 MNPs were loaded into HA-PEG-BMLs.

From SQUID analysis at room temperature, the saturation magnetization value of HA-PEG-BMLs was 16 emu/g, which is lower than that of CMNPs (65 emu/g) (Fig. 2D). This downturn in magnetization value

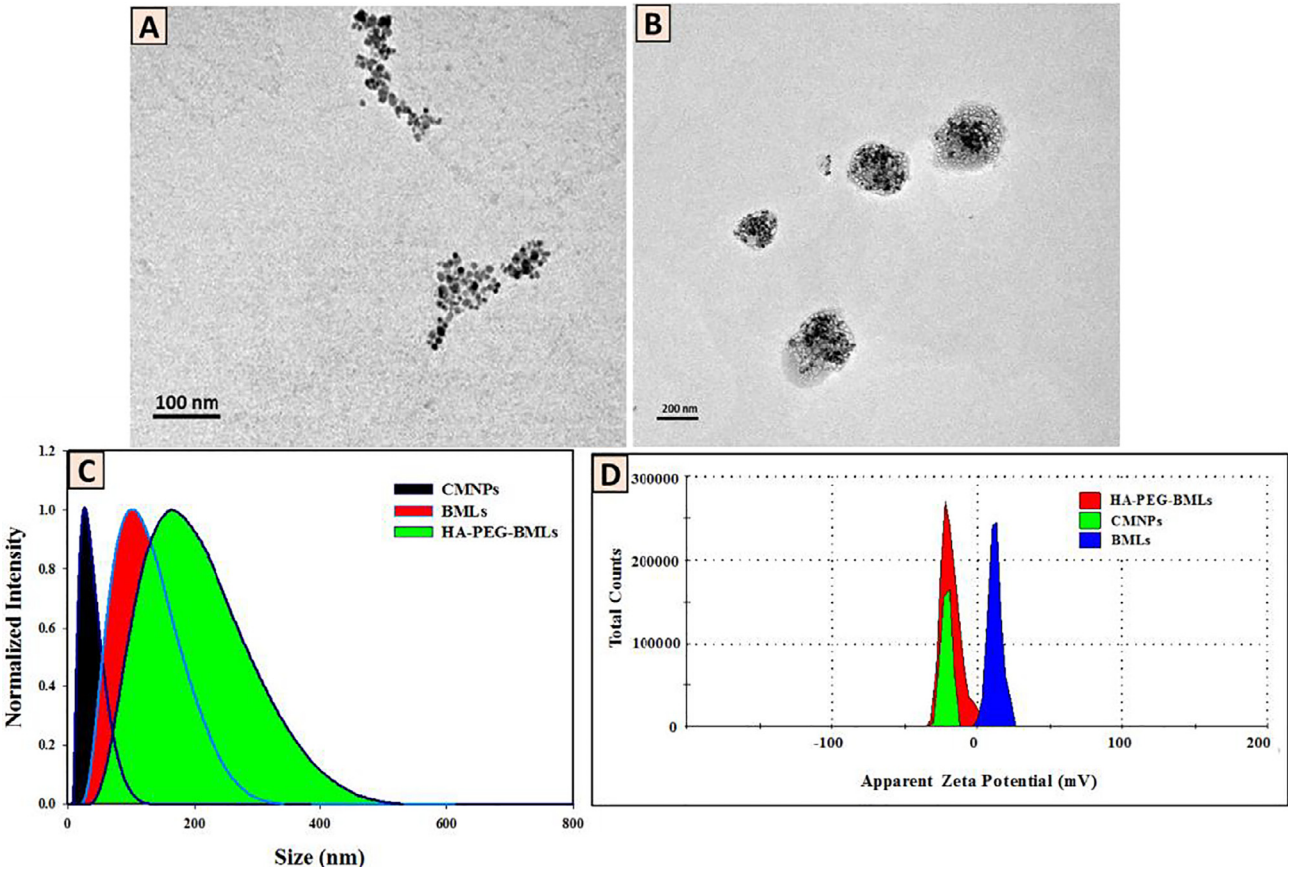

Fig. 1. TEM images of citric acid-coated magnetic nanoparticles (CMNPs) (A) and bubble-generating magnetic liposomes (BMLs) (B). Particle size (C) and zeta potential (D) distribution curves of CMNPs, BMLs and HA-PEG coated bubble-generating magnetic liposome (HA-PEG-BMLs).

Table 1
The average particle size and zeta potential of citric acid-coated magnetic nanoparticles (CMNPs), bubble-generating magnetic liposomes (BMLs) and HA-PEG coated bubble-generating magnetic liposomes (HA-PEG-BMLs). The data are expressed as means ± standard deviations (n = 4).

Sample	Particle Size (nm)	Polydispersity index	Zeta Potential (mV)
CMNPs	24 ± 3	0.213 ± 0.029	−15.4 ± 1.3
BMLs	106 ± 7*	0.278 ± 0.019*	12.0 ± 0.9*
HA-PEG-BMLs	168 ± 6*,#	0.299 ± 0.021*	−18.5 ± 1.4*,#

* $p < 0.05$ compared with CMNPs, # $p < 0.05$ compared with BMLs.

is interrelated with the encapsulation of CMNPs inside the liposome. Generally, the saturation magnetization would decrease when the CMNPs surface was covered by lipids [28]. Nonetheless, reduced saturation magnetization is expected with reduced CMNPs weight percentages in HA-PEG-BMLs, as this value is based on unit weight of samples. It should be noted that that the calculated saturation magnetization of HA-PEG-BMLs would be 16.3 emu/g, using Fe_3O_4 MNPs content determined by ICP. Thus, the diamagnetic contribution of the lipid bilayer surrounding the magnetite contributed less to the reduced saturation magnetization value than the weight effect. It should be noted even though the saturation magnetization value decreased after CMNPs were encapsulated in the liposomes, the saturation magnetization for HA-PEG-BMLs is still higher than that reported for magnetic liposomes prepared from soybean phosphatidylcholine [29]. The high magnetization value of HA-PEG-BMLs also suggested the possibility to use the nanocarrier for targeted drug delivery guided by a magnetic field. Fig. 2D also revealed the prepared CMNPs and HA-PEG-BMLs exhibited superparamagnetic property, which is characterized by the magnetization curve having no magnetic hysteresis. This endowed HA-PEG-BMLs with the important property needed for nano-sized magnetic carriers for target delivery [30].

3.2. Bubble generation, drug loading and drug release

The temperature-sensitive bubble-generating capability of liposomes was compared in Fig. 3A. For blank liposomes, the presence of bubbles was not observed at both 37 °C and 43 °C. However, in the case of bubble-generating liposome containing NH_4HCO_3, bubble formation around the liposomes could be detected by ultrasound at both temperatures with increased bubble intensity when temperature was increased from 37 °C to 43 °C. Indeed, this temperature-sensitive bubble generating capability could be related to different CO_2 bubble formation rates from decomposition of NH_4HCO_3 in the liposomes and could be explored for triggered drug release of encapsulated drug in the liposomes.

For better drug loading in the liposomes, the effect of lipid/drug ratio on DOX loading efficiency and encapsulation efficiency was studied. As shown in Fig. 3B, the encapsulation efficiency decreased with an increase in the amount of DOX used during liposome preparation, whereas the loading efficiency increased initially and then leveled off when more DOX was used. Considering both the loading efficiency and encapsulation efficiency, we optimized the preparation of HA-PEG-BMLs/DOX at a lipid/drug ratio of 1:0.05 for further studies.

Fig. 3C shows the temperature-sensitive drug release characteristics of different liposomal systems at 37 °C and 43 °C. The drug release for blank liposomes was similar at both temperatures as expected with no bubble formation. Nonetheless, in the case of bubble-generating liposomes, a distinctive temperature-dependent drug release profile could be observed. The elevation in drug release rate at 43 °C could be explained as the result of cavitation found inside the liposomes [31].

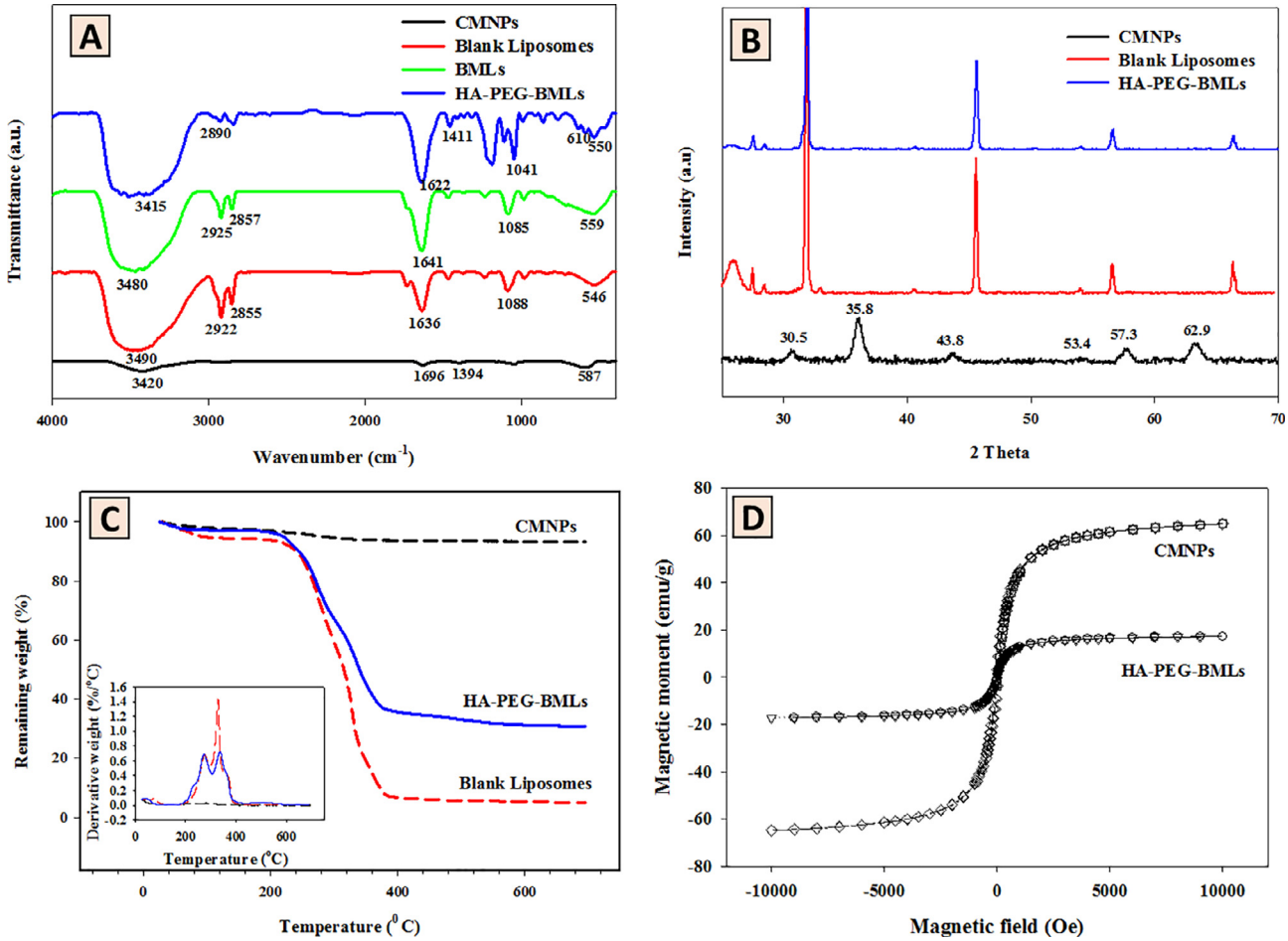

Fig. 2. Physico-chemical characterizations from Fourier transform infrared spectroscopy (FTIR) (A), X-ray diffraction (XRD) patterns (B), thermogravimetric analysis (TGA)/differential thermal analysis (DTA) (C) and superconducting quantum interference device (SQUID) magnetization curves (D).

While comparing the bubble-generating liposomes and blank liposomes at 43 °C, a faster drug release could be observed for BMLs and HA-PEG-BMLs than blank liposomes. This characteristic property is attributed to the slower decomposition behavior of NH_4HCO_3 at 37 °C, as evident from less bubble formation at this temperature than at 43 °C (Fig. 3A). On the other hand, blank liposomes at two different temperatures shows similar release properties, due to higher thermal stability of DSPC lipid used for the preparation of liposomes [32,33]. Comparing BMLs and HA-PEG-BMLs, it is also noted that the drug release rate was diminished after HA-PEG modification; indicating coating HA-PEG on liposome surface may hinder the rupture of liposomes due to the action of CO_2 bubbles. Taken together, the drug release studies confirm the effect of bubble formation on drug release and the variation in bubble intensities at different temperatures, as shown from the ultrasound images in Fig. 3A, determines the drug release rate.

3.3. Intracellular uptake and flow cytometry analysis

Confocal images revealed intracellular green fluorescence corresponding to QDs-labeled liposomes when U87 cells were exposed to BMLs and HA-PEG-BMLs for 24 h (Fig. 4). This illustrates endocytosis and the subsequent accumulation of liposomes in cell cytoplasm after internalization. In addition, the green fluorescence intensity was higher for HA-PEG-BMLs. When CD44 receptors on U87 cell surface were blocked by HA before contacting with HA-PEG-BMLs, less ligand-mediated intracellular uptake was expected for HA-PEG-BMLs [34]. Indeed, we observed drastically diminished intracellular fluorescence signal when cells were pre-treated with excess HA before contacting with HA-PEG-BMLs (Fig. 4). This difference is due to the efficient blockage of CD44 receptor on U87 cell surface with free HA in solution, which competitively inhibited the affinity of CD44 toward HA-PEG-BMLs [35]. Further confirmation of intracellular uptake through endocytosis was provided by the LysoTracker probes that could label lysosomes in living cells. As from the merged images in Fig. 4, only the HA-PEG-BMLs group shows high fluorescence intensity (yellow) corresponding to both liposomes (green) and LysoTracker (red), indicating active uptake of HA-coated liposomes by endocytosis.

The expression of CD44 on U87 cells was confirmed by flow cytometry using fluorescence-label anti-CD44 monoclonal antibody and compared with CD44 expression of normal fibroblastic cells and cancer cells. As shown in Fig. 5A, the intensity of U87 cells stained with anti-CD44 monoclonal antibody was much stronger than those of Lewis lung carcinoma (LLC1) and mouse embryonic fibroblast (MEF) cells (geometric mean intensity: 168855, 4316,1066, respectively), suggesting that U87 cells overexpress CD44 receptor on cell surface. Thus, the results of the flow cytometry support the enhanced intracellular uptake of HA-PEG-BMLs by U87 cells, as observed form the confocal images in Fig. 4. FACS analysis conducted to analyze accumulation of DOX in U87 cells also shows higher DOX accumulation when U87 cells were incubated with BMLs/DOX and HA-PEG-BMLs/DOX compared to cells treated with free DOX (Fig. 5B). The geometric mean intensities are 353, 442, 9053, 14,326 and 21,010 for control, BMLs, free DOX, BMLs/DOX and HA-PEG-BMLs/DOX, respectively. This shows that the DOX accumulation inside the cells increases when it is delivered through the liposomal nanocarrier. Most importantly, the DOX intensity was enhanced in cells treated with HA-PEG-BMLs/DOX than BMLs/DOX [36].

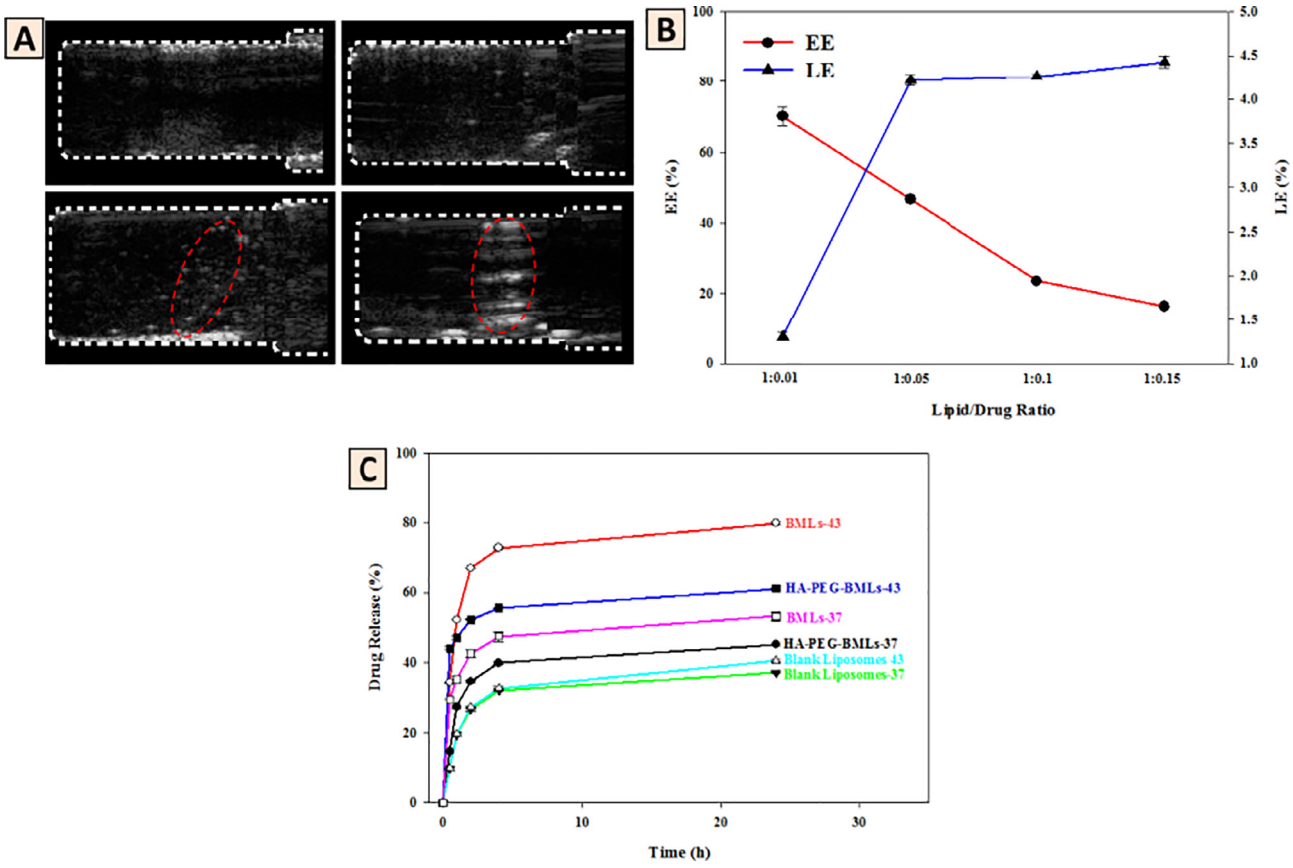

Fig. 3. (A) Ultrasound images of blank liposomes (top) and bubble-generating liposomes (BMLs) (bottom) at 37 °C (left) and 43 °C (right). CO_2 bubbles were marked with red circles. (B) The effect of lipid/drug ratio during the preparation of drug-loaded liposomes on loading efficiency (LE) and encapsulation efficiency (EE) of DOX (n = 4). (c) The drug release profiles of blank liposomes and bubble-generating liposomes (BMLs and HA-PEG-BMLs) at 37 °C and 43 °C (n = 4).

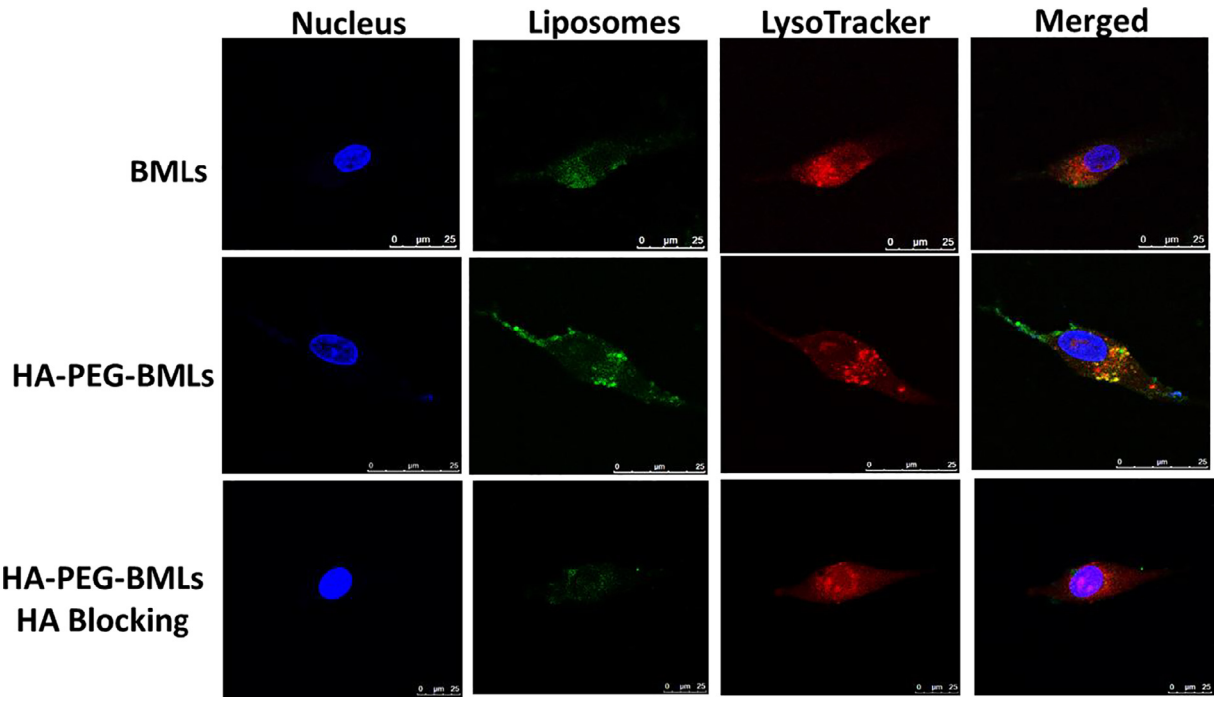

Fig. 4. Intracellular uptake studies of BMLs and HA-PEG-BMLs by U87 cells as examined by confocal microscopy after 24 h. Liposomes were labelled with QDs (green), nuclei were counter stained with Hoechst (blue) and LysoTracker probes was used to label lysosomes (red). Bar = 25 μm.

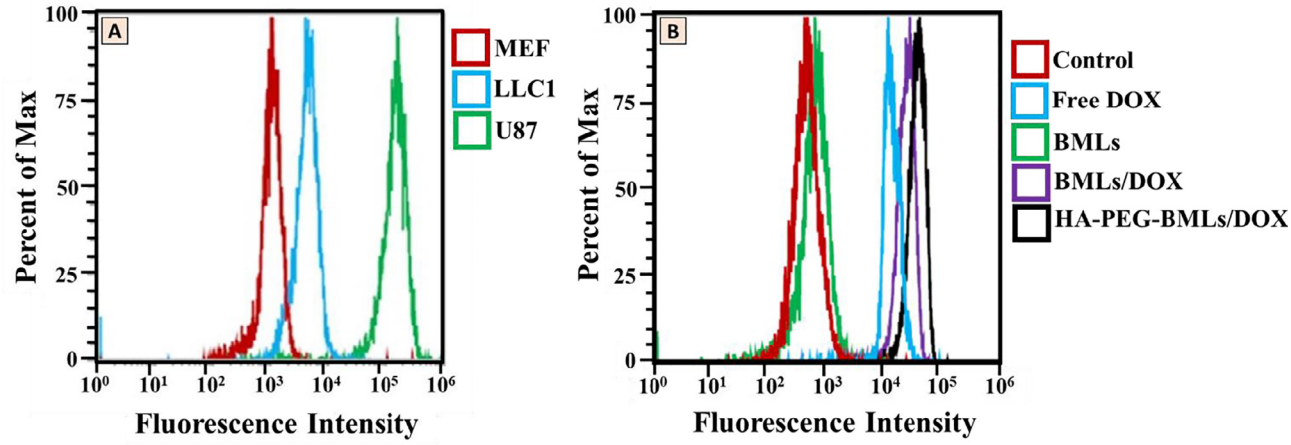

Fig. 5. (A) Flow cytometry analysis for identification of CD44 surface marker in mouse embryonic fibroblast (MEF), Lewis lung carcinoma (LLC1) and U87 cells and (B) flow cytometry analysis of DOX in U87 cells.

This result substantiates the presence and functioning of CD44 receptors on the surface of U87 cells, which could bind to HA-PEG on HA-PEG-BMLs to critically enhance the uptake of HA-PEG-BMLs/DOX for cancer therapy.

3.4. Magnetic targeting

For magnetic targeting effect, U87 cells were treated with HA-PEG-BMLs/DOX in a 24-well culture plate that has a small permanent magnet placed at the center of each well. The LIVE/DEAD staining images indicated few viable cells (green) could be identified in the magnetically targeted area (enclosed by the blue dotted line) while abundant dead cells (red) were found in the same area (Fig. 6A). The percentages of live and dead cells were calculated to be 12% and 88%, respectively. In contrast, most of the cells outside this area (outside of the blue dotted line) were viable with 92% live cells and 8% dead cells. Furthermore, it could be also confirmed that most live cells in the targeted area and most dead cells in the non-targeted area are found close to the boundary of the magnetically targeted area (i.e. blue dotted line). This indicates DOX-loaded magnetic liposomes could be magnetically guided by a permanent magnetic field for targeted DOX delivery [37]. On the contrary, in the absence of magnetic targeting, HA-PEG-BMLs/DOX would distribute randomly in the well, which resulted in nonspecific cell death as revealed from Fig. 6B with almost equal percentage of live (55%) and dead (45%) cells. Therefore, HA-PEG-BMLs/DOX could therefore be magnetically guided to the tumor site with a magnetic field for specific killing of cells at the targeting site with minimum side effects toward surrounding healthy cells. Combining with HA ligand-directed targeting, HA-PEG-BMLs is a promising nanocarrier for dual targeted drug delivery of DOX.

3.5. In vitro cytotoxicity

In vitro cytotoxicity study was first conducted to evaluate the biocompatibility of the nanocarrier. The result shown in Fig. 7A indicates no appreciable toxicity for all liposomal formulation without DOX, demonstrating high biocompatibility of the prepared liposomes (Fig. 7A). Nonetheless, both BMLs and HA-PEG-BMLs show lower cell viability compared to blank liposomes, which could be ascribed to the formation, growth, and collapse of CO_2 bubbles, generated from the decomposition of NH_4HCO_3 inside the liposomes. Furthermore, BMLs and HA-PEG-BMLs, but not blank liposomes, showed significantly lower cytotoxicity at 37 °C than at 43 °C. This result is consistent with the observation of bubble formation in Fig. 3A, although bubble formation

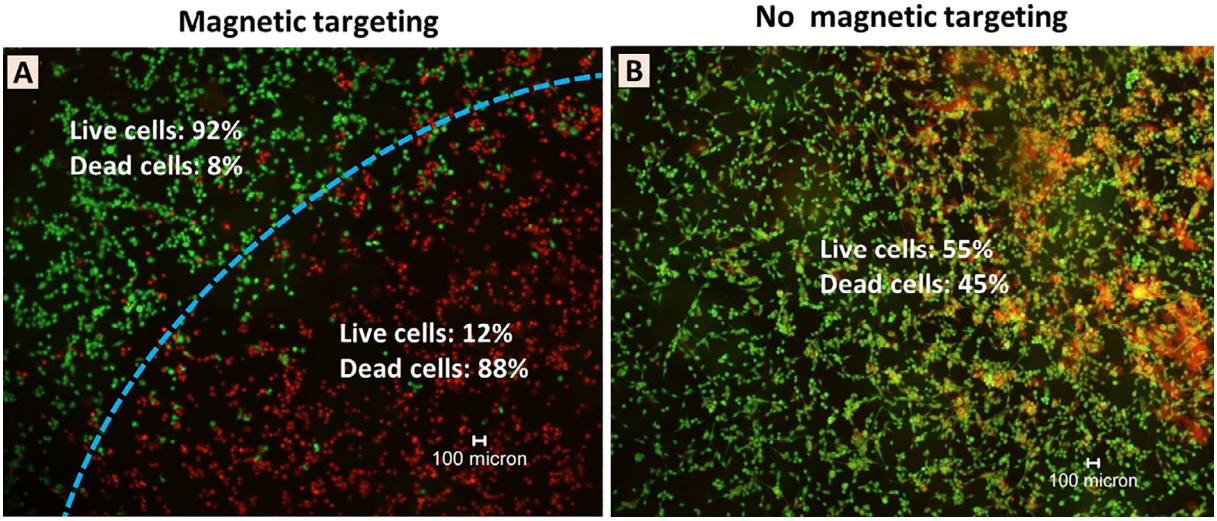

Fig. 6. The effect of magnetic guidance on distribution of live and dead cells after U87 cells were treated with HA-PEG-BMLs/DOX for 24 h with or without magnetic targeting. The cells were analyzed by LIVE/DEAD assays and examined under a fluorescence microscope where green and red fluorescence represent live and dead cells, respectively. The blue dotted line indicates the boundary of the magnetically targeted area using a permanent magnet. Bar = 100 μm.

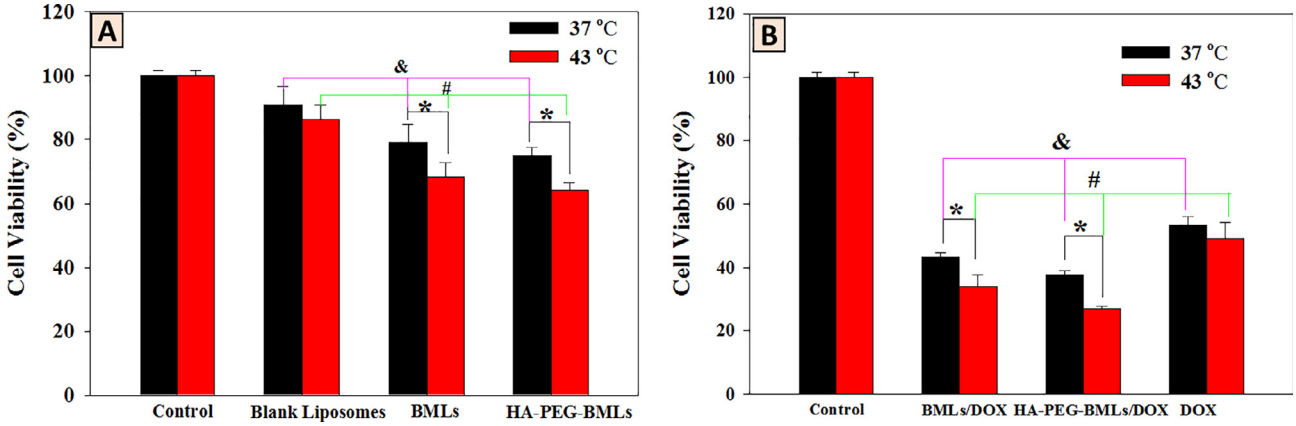

Fig. 7. Biocompatibility (A) and cytotoxicity (B) of various liposomal formulations at 37 °C and 43 °C (n = 6). The concentration of DOX was fixed at 10 μg/mL DOX. $^{*}p < 0.05$ compared with 37 °C in each group, $^{\&}p < 0.05$ among groups at 37 °C, $^{\#}p < 0.05$ among groups at 43 °C.

started from 37 °C; increased bubble intensity was observed at 43 °C. This phenomenon is expected to induce more cavitation and influence cell viability. On the other hand, as modification of BMLs with HA-PEG plays a significant role in enhancing intracellular uptake, HA-PEG-BMLs showed significantly lower cell viability than BMLs at both temperatures. It is worth pointing out that most normal tissues remain undamaged following treatment for 1 h at temperatures up to 43 °C [6]. This feature makes the new liposomal system potentially safe for clinical use.

The cytotoxicity of the DOX-loaded liposomes was studied at 37 °C and 43 °C and compared with free DOX at the same drug concentration (Fig. 7B). Compared with DOX, BMLs/DOX and HA-PEG-BMLs/DOX were found to be significantly more cytotoxic to cancer cells at both temperatures, indicating their efficacy for cancer therapy. The enhanced cytotoxicity is also in line with the higher intracellular DOX concentration found from flow cytometry (Fig. 5B) when the drug is delivered through liposomes. For both BMLs/DOX and HA-PEG-MLP/BMLs, treatment at 43 °C shows predominantly higher cytotoxicity when compared to 37 °C due to the higher bubble intensity and elevated drug release at 43 °C (Fig. 3A and C). As expected, HA-PEG-BMLs/DOX showed the highest cytotoxicity against U87 among all DOX-treated groups due to ligand-mediated enhanced intracellular uptake, which gave the highest intracellular DOX concentration from flow cytometry analysis (Fig. 5B).

We further used flow cytometry to confirm the cytotoxicity of BMLs/DOX and HA-PEG-BMLs/DOX was induced by apoptosis. The cells were stained with Annexin V/PI to quantify live, early apoptotic, late apoptotic and necrotic cells by flow cytometry analysis according to differences in plasma membrane integrity and permeability. The percentage of necrotic (Q1), late apoptotic (Q2), early apoptotic (Q4) and live cells (Q3) are shown in Fig. 8. The flow cytometry data confirm cell death occurred mainly from early and late apoptosis associated with DOX [38]. Similar to the result obtained from the MTT assay (Fig. 7), blank liposomes show high biocompatibility with U87 cells. For BMLs, increase in temperature from 37 °C to 43 °C results in formation of more bubbles, which leads to more cavitation and higher cell apoptosis rate and live cells decrease from 79.0% to 71.0%. When this cavitation effect is combined with DOX release for BMLs/DOX, the live cells further decrease from 79.0% to 64.1% at 37 °C and from 71.0% to 62.1% at 43 °C, as the bubble can rupture liposome membrane for drug release along with cell rupture. This results in the release of more DOX intracellularly and enhances the cytotoxicity. BMLs/DOX treatment also results in less live cells than free DOX, which is 69.5% (37 °C) and 65.0% (43 °C). For HA-PEG-BMLs/DOX, enhanced cytotoxicity was expected due to ligand-mediated intracellular uptake of HA-PEG-BMLs through interaction of HA with CD44 receptor on U87 cell surface. Although the drug release profiles indicate the drug release percentage of HA-PEG-BMLs/DOX was less than that of BMLs/DOX at both

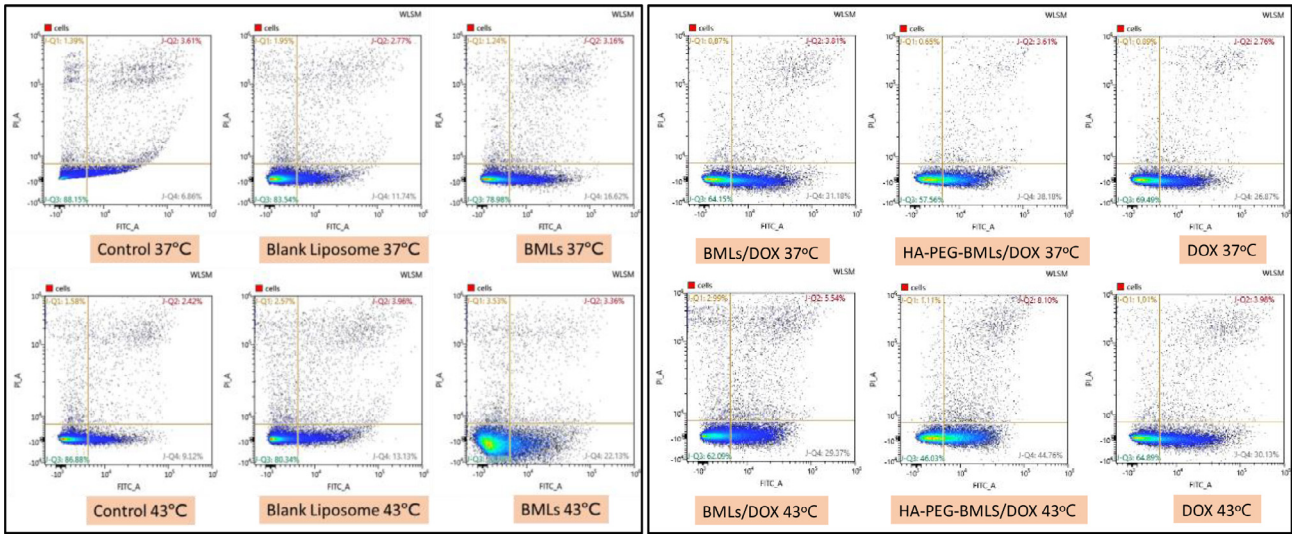

Fig. 8. The flow cytometry analysis of apoptotic and necrotic cells by Annexin V/PI staining (Q1: necrotic; Q2: late apoptotic; Q3: live; Q4: early apoptotic) after 24 h incubation with free DOX, liposomes or DOX-loaded liposomes at 37 °C and 43 °C. The concentration of DOX was fixed at 10 μg/ml.

temperatures (Fig. 3C), we could still find much less live cells for HA-PEG-BMLs/DOX than BMLs/DOX (57.6% vs 64.1% at 37 °C; 46.0% vs 62.1% at 43 °C) due to enhanced intracellular uptake of the former. Taken together, the results reveal the combinatory effect of bubble generation and DOX release for cell cytotoxicity, which could be further enhanced at higher temperature.

The results obtained from in vitro experiments suggest the effectiveness of HA-PEG-BMLs/DOX in cancer therapy. It should be noted that hyperthermia-based drug release could be conveniently accomplished under an applied alternating magnetic field (AMF), which works based on principles of Brownian relaxation and Neel effect [39]. The MNPs in the liposomes will therefore generate hyperthermia effect in the presence of AMF for drug release, which could be translated into a drug delivery system in vivo using bubble-generating magnetic liposomes. This will provide a remotely controlled drug delivery system using HA-PEG-BMLs/DOX for cancer therapy in vivo. The in vitro cytotoxicity study endorses intravenous administration of HA-PEG-BMLs/DOX, which exhibits the highest cytotoxicity under hyperthermia condition at 43 °C, for targeted delivery of DOX to cancer cells, followed by AMF treatment to induce hyperthermia for future translational study in vivo.

4. Conclusion

We successfully prepared and characterized bubble-generating magnetic liposomes in this study and demonstrated dual targeted DOX delivery was possible through magnetic targeting (with encapsulated CMNPs) and ligand-mediated intracellular uptake (by interaction of HA with CD44). We confirmed the modification of BMLs with HA-PEG is a promising strategy for the enhanced intracellular uptake of the liposomal nano-carrier by cancer cells, which elevated DOX concentration intracellularly in the cancer cells for enhanced cytotoxicity. The bubble-generating liposomes, BMLs and HA-PEG-BMLs, provide a powerful tool for temperature-sensitive bubble generation, and temperature-responsive DOX release for killing U87 cancer cells. Hyperthermia-based bubble generation followed by triggered drug release render HA-PEG-BMLs/DOX to be a promising nano-carrier for dual targeted cancer therapy.

Acknowledgements

The financial assistance was provided by grants from the Ministry of Science and Technology, Taiwan (106-2221-E-182-056-MY3) and Chang Gung Memorial Hospital (BMRP 249, CMRPD2G0081 and CMRPD2G0082). The Microscope Core Laboratory in Chang Gung Memorial Hospital, Linkou is acknowledged for the confocal microscopy study.

References

[1] E.Y. Chuang, C.C. Lin, K.J. Chen, D.H. Wan, K.J. Lin, Y.C. Ho, P.Y. Lin, H.W. Sung, A FRET-guided, NIR-responsive bubble-generating liposomal system for in vivo targeted therapy with spatially and temporally precise controlled release, Biomaterials 93 (2016) 48–59.
[2] S.-L. Huang, Liposomes in ultrasonic drug and gene delivery, Adv. Drug Deliv. Rev. 60 (2008) 1167–1176.
[3] R. Mo, T. Jiang, R. DiSanto, W. Tai, Z. Gu, ATP-triggered anticancer drug delivery, Nature Commun. 5 (2014) 3364.
[4] V.P. Torchilin, Recent advances with liposomes as pharmaceutical carriers, Nat. Rev. Drug Discov. 4 (2005) 145–160.
[5] Z. Deng, M. Tang, L. Zhao, Y. Long, Z. Wen, Y. Cheng, H. Zheng, Targeted H(+)-triggered bubble-generating nanosystems for effective therapy in cancer cells, Colloids Surf. B 160 (2017) 207–214.
[6] M.F. Chung, K.J. Chen, H.F. Liang, Z.X. Liao, W.T. Chia, Y. Xia, H.W. Sung, A liposomal system capable of generating CO_2 bubbles to induce transient cavitation, lysosomal rupturing, and cell necrosis, Ang. Chem. Int. Ed. 51 (2012) 10089–10093.
[7] D.A. Balazs, W. Godbey, Liposomes for use in gene delivery, J. Drug Deliv. 2011 (2011) 326497.
[8] M.B. Yatvin, J.N. Weinstein, W.H. Dennis, R. Blumenthal, Design of liposomes for enhanced local release of drugs by hyperthermia, Science 202 (1978) 1290–1293.
[9] A. Akbarzadeh, R. Rezaei-Sadabady, S. Davaran, S.W. Joo, N. Zarghami, Y. Hanifehpour, M. Samiei, M. Kouhi, K. Nejati-Koshki, Liposome: classification, preparation, and applications, Nanoscale Res. Lett. 8 (2013) 102.
[10] R. Fernández-Pacheco, C. Marquina, J. Gabriel Valdivia, M. Gutiérrez, M. Soledad Romero, R. Cornudella, A. Laborda, A. Viloria, T. Higuera, A. García, J.A.G. de Jalón, M. Ricardo Ibarra, Magnetic nanoparticles for local drug delivery using magnetic implants, J. Mag. Mag. Mater. 311 (2007) 318–322.
[11] M. De Cuyper, M. Joniau, Magnetoliposomes. Formation and structural characterization, Eur. Biophys. J. 15 (1988) 311–319.
[12] H.-L. Hsu, J.-P. Chen, Preparation of thermosensitive magnetic liposome encapsulated recombinant tissue plasminogen activator for targeted thrombolysis, J. Mag. Mag. Mater. 427 (2017) 188–194.
[13] J. Giri, S. Guha Thakurta, J. Bellare, A. Kumar Nigam, D. Bahadur, Preparation and characterization of phospholipid stabilized uniform sized magnetite nanoparticles, J. Mag. Mag. Mater. 293 (2005) 62–68.
[14] I.K. Kwon, S.C. Lee, B. Han, K. Park, Analysis on the current status of targeted drug delivery to tumors, J. Control. Release 164 (2012) 108–114.
[15] D. Peer, J.M. Karp, S. Hong, O.C. Farokhzad, R. Margalit, R. Langer, Nanocarriers as an emerging platform for cancer therapy, Nature Nanotechnol. 2 (2007) 751.
[16] Y.-S. Huang, Y.-J. Lu, J.-P. Chen, Magnetic graphene oxide as a carrier for targeted delivery of chemotherapy drugs in cancer therapy, J. Mag. Mag. Mater. 427 (2017) 34–40.
[17] L.Y. Bourguignon, M. Shiina, J.J. Li, Hyaluronan-CD44 interaction promotes oncogenic signaling, microRNA functions, chemoresistance, and radiation resistance in cancer stem cells leading to tumor progression, Adv. Cancer Res. 123 (2014) 255–275.
[18] A. Perschl, J. Lesley, N. English, I. Trowbridge, R. Hyman, Role of CD44 cytoplasmic domain in hyaluronan binding, Eur. J. Immunol. 25 (1995) 495–501.
[19] M. Racuciu, D.E. Creanga, A. Airinei, Citric-acid-coated magnetite nanoparticles for biological applications, Eur. Phys. J. E, Soft Matter. 21 (2006) 117–121.
[20] A. Hardiansyah, L.-Y. Huang, M.-C. Yang, T.-Y. Liu, S.-C. Tsai, C.-Y. Yang, C.-Y. Kuo, T.-Y. Chan, H.-M. Zou, W.-N. Lian, C.-H. Lin, Magnetic liposomes for colorectal cancer cells therapy by high-frequency magnetic field treatment, Nanoscale Res. Lett. 9 (2014) 497.
[21] K. Moriyama, T. Ooya, N. Yui, Hyaluronic acid grafted with poly(ethylene glycol) as a novel peptide formulation, J. Control. Release 59 (1999) 77–86.
[22] A. Cern, A. Golbraikh, A. Sedykh, A. Tropsha, Y. Barenholz, A. Goldblum, Quantitative structure – property relationship modeling of remote liposome loading of drugs, J. Control. Release 160 (2012) 147–157.
[23] K.-J. Chen, E.-Y. Chaung, S.-P. Wey, K.-J. Lin, F. Cheng, C.-C. Lin, H.-L. Liu, H.-W. Tseng, C.-P. Liu, M.-C. Wei, C.-M. Liu, H.-W. Sung, Hyperthermia-mediated local drug delivery by a bubble-generating liposomal system for tumor-specific chemotherapy, ACS Nano 8 (2014) 5105–5115.
[24] T. Neuberger, B. Schöpf, H. Hofmann, M. Hofmann, B. von Rechenberg, Superparamagnetic nanoparticles for biomedical applications: Possibilities and limitations of a new drug delivery system, J. Mag. Mag. Mater. 293 (2005) 483–496.
[25] H. Salehizadeh, E. Hekmatian, M. Sadeghi, K. Kennedy, Synthesis and characterization of core-shell Fe_3O_4-gold-chitosan nanostructure, J. Nanobiotechnol. 10 (2012) 3.
[26] A. Goodarzi, Y. Sahoo, M.T. Swihart, P.N. Prasad, Aqueous ferrofluid of citric acid coated magnetite particles, MRS Proceedings 789 (2011) N6.6.
[27] J.A. Alkrad, Y. Merstani, R.H. Neubert, New approaches for quantifying hyaluronic acid in pharmaceutical semisolid formulations using HPLC and CZE, J. Pharm. Biomed. Anal. 30 (2002) 913–919.
[28] M. Mahmoudi, S. Sant, B. Wang, S. Laurent, T. Sen, Superparamagnetic iron oxide nanoparticles (SPIONs): development, surface modification and applications in chemotherapy, Adv. Drug Deliv. Rev. 63 (2011) 24–46.
[29] S. Garcia-Jimeno, E. Escribano, J. Queralt, J. Estelrich, Magnetoliposomes prepared by reverse-phase followed by sequential extrusion: characterization and possibilities in the treatment of inflammation, Int. J. Pharm. 405 (2011) 181–187.
[30] A.K. Gupta, A.S.G. Curtis, Surface modified superparamagnetic nanoparticles for drug delivery: Interaction studies with human fibroblasts in culture, J. Mater. Sci. Mater. Med. 15 (2004) 493–496.
[31] T. Ta, E. Bartolak-Suki, E.J. Park, K. Karrobi, N.J. McDannold, T.M. Porter, Localized delivery of doxorubicin in vivo from polymer-modified thermosensitive liposomes with MR-guided focused ultrasound-mediated heating, J. Control. Release 194 (2014) 71–81.
[32] C.M. González-Henríquez, V.A. Villegas-Opazo, D.H. Sagredo-Oyarce, M.A. Sarabia-Vallejos, C.A. Terraza, Thermal response analysis of phospholipid bilayers using ellipsometric techniques, Biosensors 7 (2017) 34.
[33] N. Kucerka, M.P. Nieh, J. Katsaras, Fluid phase lipid areas and bilayer thicknesses of commonly used phosphatidylcholines as a function of temperature, Biochim. Biophys. Acta 2011 (1808) 2761–2771.
[34] S.L. Hayward, C.L. Wilson, S. Kidambi, Hyaluronic acid-conjugated liposome nanoparticles for targeted delivery to CD44 overexpressing glioblastoma cells, Oncotarget 7 (2016) 34158–34171.
[35] L. Mo, J.G. Song, H. Lee, M. Zhao, H.Y. Kim, Y.J. Lee, H.W. Ko, H.-K. Han, PEGylated hyaluronic acid-coated liposome for enhanced in vivo efficacy of sorafenib via active tumor cell targeting and prolonged systemic exposure, Nanomed. Nanotechnol. 14 (2018) 557–567.
[36] Y.T. Fong, C.H. Chen, J.P. Chen, Intratumoral delivery of doxorubicin on folate-conjugated graphene oxide by in-situ forming thermo-sensitive hydrogel for breast cancer therapy, Nanomaterials 7 (2017) 388.
[37] Y.J. Lu, K.C. Wei, C.C. Ma, S.Y. Yang, J.P. Chen, Dual targeted delivery of doxorubicin to cancer cells using folate-conjugated magnetic multi-walled carbon nanotubes, Colloids Surf. B 89 (2012) 1–9.
[38] H. Mizutani, S. Tada-Oikawa, Y. Hiraku, M. Kojima, S. Kawanishi, Mechanism of apoptosis induced by doxorubicin through the generation of hydrogen peroxide, Life Sci. 76 (2005) 1439–1453.
[39] C.S. Kumar, F. Mohammad, Magnetic nanomaterials for hyperthermia-based therapy and controlled drug delivery, Adv. Drug Deliv. Rev. 63 (2011) 789–808.